Adsorptive oxidation of sulfides catalysed by δ-MnO_2 decorated porous graphitic carbon composite

Edathil, Anjali Achazhiyath; Kannan, Pravin; Banat, Fawzi

Published in:
Environmental Pollution

Link to article, DOI:
10.1016/j.envpol.2020.115218

Publication date:
2020

Document Version
Peer reviewed version

Journal Pre-proof

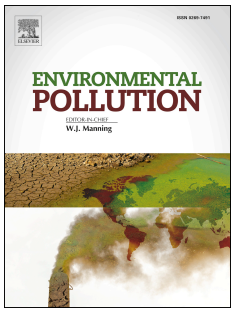

Adsorptive oxidation of sulfides catalysed by δ-MnO_2 decorated porous graphitic carbon composite

Anjali Achazhiyath Edathil, Pravin Kannan, Fawzi Banat

PII: S0269-7491(20)34318-9

DOI: https://doi.org/10.1016/j.envpol.2020.115218

Reference: ENPO 115218

To appear in: *Environmental Pollution*

Received Date: 29 May 2020

Revised Date: 2 July 2020

Accepted Date: 7 July 2020

Please cite this article as: Edathil, A.A., Kannan, P., Banat, F., Adsorptive oxidation of sulfides catalysed by δ-MnO_2 decorated porous graphitic carbon composite, *Environmental Pollution* (2020), doi: https://doi.org/10.1016/j.envpol.2020.115218.

CRediT author statement

Anjali Edathil: Methodology, Investigation, Visualization, Writing-Reviewing & Editing

Pravin Kannan: Writing – Original draft, Reviewing & Editing, Formal analysis, validation

Fawzi Banat: Conceptualization, Writing-Reviewing & Editing, Supervision, Project administration

Adsorptive oxidation of sulfides catalysed by δ-MnO_2 decorated porous graphitic carbon composite

Anjali Achazhiyath Edathil, Pravin Kannan*, Fawzi Banat*

Department of Chemical Engineering, Khalifa University, Abu Dhabi, United Arab Emirates

Graphical Abstract

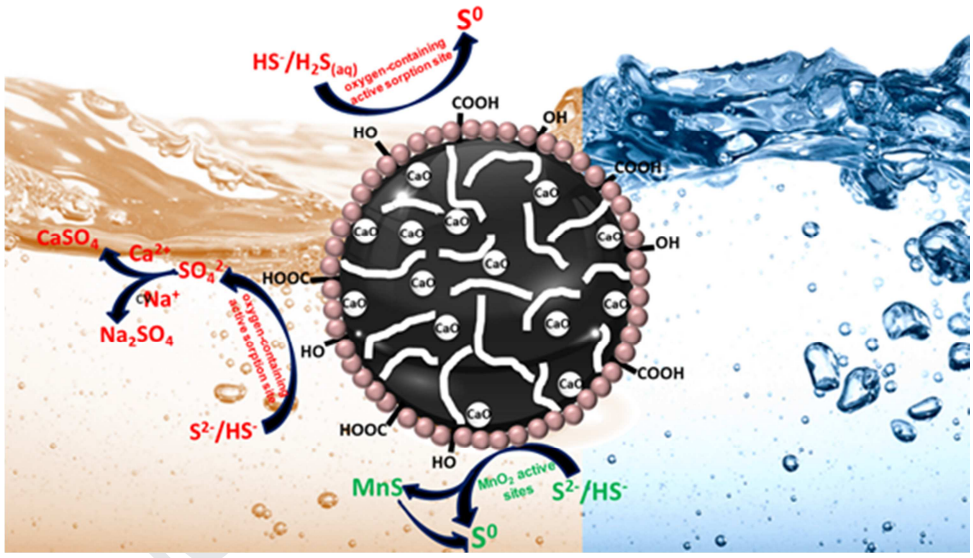

Environmentally benign bio adsorbent for sulfide removal

Adsorptive oxidation of sulfides catalysed by δ-MnO_2 decorated porous graphitic carbon composite

Anjali Achazhiyath Edathil [a,b], Pravin Kannan [*,b], Fawzi Banat [b]

[a] – *National Center for Nano Fabrication and Characterization, DTU Nanolab, Technical University of Denmark, 2800, Kgs. Lyngby, Denmark*

[b] - *Department of Chemical Engineering, Khalifa University, P.O. Box 127788, Abu Dhabi, United Arab Emirates*

[*] Corresponding author. *Tel*.: +971 26075198

Email addresses: pravin.kannan@ku.ac.ae

Abstract

Removal of dissolved sulfide contaminants from aqueous model solution using bio-derived porous graphitic carbon (PGC) impregnated with δ-MnO_2 was investigated. The composite adsorbent was synthesized using the chemical wet deposition method wherein MnO_2 was deposited on carbon walls through an in-situ reaction between permanganate and ethanol. Formation of transition metal oxide of manganese in the form of birnessite nanoparticles on interconnected PGC cell structure was confirmed by transmission electron microscopy, scanning electron microscopy, elemental analysis, and X-Ray diffraction characterization studies. The composite nanomaterial was tested for sulfide removal from aqueous solution at various conditions, including the pH, adsorbent dosage, initial solution concentration, and contact time. Adsorption results demonstrated an excellent adsorption capacity of ca. 90% within 20 minutes of contact time at 298 K. Equilibrium data collected from batch adsorption experiments fitted well with the Langmuir isotherm model (K_L = 190 L/mg; R^2 = 0.99). The maximum adsorption capacity of the composite was estimated as 526.3 mg S^{2-}/g at highly alkaline conditions compared to ca. 340 mg/g for a δ-MnO_2 adsorbent. Adsorptive oxidation of sulfides on composite MnO_2-PGC adsorbent was found to be controlled by the chemisorption process in accordance with the pseudo-second-order reaction model. Characterization of spent adsorbents revealed that sulfide was removed through adsorptive oxidation resulting in the formation of agglomerated particles of metal sulfate complexes and elemental sulfur. Analysis of reaction mechanism revealed that both MnO_2 and PGC played a role in the adsorptive oxidation of sulfides to $CaSO_4$ and elemental sulfur.

Capsule: δ-MnO_2/PGC nanocomposite synthesized using a facile in-situ wet deposition technique exhibited superior sulfide uptake capacity

Keywords: δ-MnO_2, adsorption, Sulfide wastewater, Alginate, Porous graphitic carbon

1. Introduction

Effluents released from coke and steel industries, pulp and paper, petroleum refinery, municipal wastewater treatment plants, and animal husbandries have been found to contain dissolved hydrogen sulfide (H_2S), bisulfides (HS^-), and sulfide ions (S^{2-}) (Kociolek-Balawejder and Wilk, 2011) which are often grouped together and referred as "sulfides". Reuse of sulfide contaminated water for industrial applications is severely restricted due to the undesired reaction of sulfide components with metal and metal oxides. This results in the formation of metal sulfides in which induces sulfide corrosion of pipelines and processing equipment. The dissolved sulfide compounds in wastewater can also be released to the gaseous phase as H_2S, thereby compounding the adverse environmental effects of sulfides even at lower concentrations (Wilk et al., 2020). With the increase of sour gas fields in and around the middle eastern countries, generation and subsequent release of sulfide contaminated wastewater pose a serious environmental concern. Thus, removal of sulfide metal ions from refinery wastewater, preferably to a concentration below 0.2 ppm, is critical not only for safer discharge into aquatic bodies (Vaiopoulou et al., 2005), but also to develop sustainable industrial practices in refinery plant operations.

The presence and distribution of different ionic species of hydrogen sulfide in wastewater primarily depend on solution pH. Thompson et al. (1995) reported that at lower pH values (5-6), the predominant sulfide species remains to be aqueous hydrogen sulfide (H_2S_{aq}), and with a slight increase in pH (7-9), the solution primarily contains bisulfides (HS^-) along with sulfide (S^{2-}) ions. However, at higher solution pH (>10), the only sulfur species present in the solution are the reduced species of sulfur, S^{2-} ions.

Removal of sulfide ions from wastewater could be achieved by various techniques, including filtration after liming and recycling (Artiga et al., 2005), neutralization (Tamersit and Bouhidel, 2020), recuperation of sulfides and reuse (Komanowsky et al., 1984), precipitation of sulfides by iron salts (Chen et al., 2018; Firer et al., 2008), oxidation by oxidizing agents with or without catalysts (Heideman et al., 1984), and biological detoxification of sulfides (Marais et al., 2020; Mestrinelli et al., 2016). Among these techniques, direct oxidation of sulfides by oxidizers has been researched using different oxidizing agents like H_2O_2, $KMnO_4$, and ozone. Although H_2O_2 is the widely used oxidizer in practice, direct removal of sulfides from water using $KMnO_4$ is also well-known (Cadena and Peters, 1988; Dohnalek and FitzPatrick, 1983; Willey et al., 1964).

Sulfide oxidation reaction by $KMnO_4$ can follow different complex pathways depending on the conditions encountered. For example, in the absence of oxygen, permanganate directly oxidizes hydrogen sulfide. On the contrary, in aerobic systems, sulfide oxidation proceeds by reaction with oxygen to form various sulfur compounds in addition to MnO_2. As the reaction continues, MnO_2 acts as an oxygen-transfer catalyst and assists in further sulfide oxidation. However, this process converts sulfides into elemental sulfur in addition to other by-products like agglomerated MnO_2 that needs to be subsequently removed by filtration, thereby increasing the energy demand. Yao et al. demonstrated that the rate of sulfide oxidation in seawater is significantly enhanced by δ-MnO_2 through the formation of surface complexes (Yao and Millero, 1993). The spent MnO_2, and the oxidized MnOOH are insoluble in alkaline medium and hence favours ease of separation from wastewater (Valeika et al., 2006).

Adsorption has gained increased attention due to lower process energy demand and substantial capability in removing trace quantities of contaminants, including heavy metals (Burakov et al., 2018), and sulfide ions (Bono et al., 2016; Li et al., 2017; Soto et al., 2011) from

wastewater. Traditionally, activated carbon synthesized from coal and various biomass materials, mainly cellulosic and microbial origin (Gupta et al., 2015; Lu et al., 2020; Suhas et al., 2016) has been employed as adsorbents due to its high porosity and surface area. However, large-scale treatment using activated carbon remains challenging because of the low selectivity of carbon towards sulfide ions. Different carbon materials like porous carbon, carbon nanotubes and fullerene have been extensively used for advanced treatment of wastewaters (Gupta and Saleh, 2013). Recently, graphene-based material has been successfully utilized as an adsorbent in the field of nano sciences (Amiri et al., 2018; Mondal et al., 2018), specifically for environmental remediation (Achazhiyath Edathil et al., 2019; La et al., 2017). This led to the development of carbon-based composite adsorbents surface functionalized with various metal oxides that cater to the removal of specific contaminants. Anchoring δ-MnO_2 on carbon structures would facilitate separation of spent adsorbents, in addition to providing enhanced adsorption capacity and improved mechanical and chemical stability. Many techniques have been proposed in the literature for in-situ synthesis of δ-MnO_2, including precipitation using $KMnO_4$ and different alcohols (Subramanian et al., 2008). Detailed synthesis studies conducted by Subramanian et al (Subramanian et al., 2008) revealed that the morphology and the oxidized state of Mn deposited on carbon walls depends on the type of alcohol used. Using the surface manoeuvring property of alcohols, nanostructured δ-MnO_2 is formed by nucleation, aggregation and coalescence of particles.

During recent times, the superior physical properties of porous graphitic carbon have been exploited for numerous industrial applications, specifically as adsorption and separation media (Chai et al., 2012; Gokulakrishnan et al., 2011; Stein et al., 2009). Novel synthesis techniques have focussed on the design of porous carbon structures with surface functionalization, offering increased adsorption capacity, high selectivity, and low density. A

substantial amount of research has focussed on developing sustainable wastewater treatment techniques by employing bio-derived porous carbon material. Among numerous bio-derived carbon, sodium alginate derived from brown seaweed has shown great potential as a carbon precursor for various energy and environmental applications (Srinivasan, 2013). Our previous work investigated sulfide removal from aqueous solution using porous graphitic carbon synthesized from alginate, and the results confirmed the enhanced adsorptive capacity of PGC for sulfides (Edathil et al., 2017). In the present study, the superior oxidative property of δ-MnO_2 in conjunction with highly selective and enhanced adsorptive capacity of porous graphitic carbon derived from a natural polymer, sodium alginate, is realized through MnO_2-PGC composite adsorbent. In-situ synthesis of δ-MnO_2 using $KMnO_4$ and ethanol on porous graphitic carbon through a wet chemical deposition technique has been demonstrated. The complex interconnected hierarchical porous carbon structure evenly distributed with δ-MnO_2 could be expected to facilitate electron transfer and oxidize sulfides to elemental sulfur and sulfates. The efficacy and suitability of the adsorbent are evaluated by determining the removal efficiency and maximum uptake capacity of sulfide species. As the composite adsorbent is synthesized from bio derived PGC, the applicability of the adsorbent for sulfide removal from aqueous solution is further encouraged.

2. EXPERIMENTAL SECTION

2.1. Materials

Alginic acid calcium salt, potassium permanganate, and ethanol were purchased from Sigma Aldrich, USA, and sodium sulfide ($Na_2S·9H_2O$) was obtained from Fisher Scientific. All chemicals were of analytical grade and hence used without further purification. Deionized water was used in the preparation and dilution of all solutions. Sulfide model solutions were prepared

by dissolving crystals of $Na_2S \cdot 9H_2O$ in deionized water and passing nitrogen gas to avoid oxidation of sulfide. Various concentrations of sulfide solutions were prepared by further diluting the prepared model solution with deionized water.

2.2. Synthesis of PGC, MnO_2, and MnO_2-PGC Composites

First, porous graphitic carbon (PGC) was synthesized by annealing and subsequent carbonization of alginic acid calcium salt as described in our earlier work (Edathil et al., 2017). To prepare the MnO_2-PGC composites, equal quantities of $KMnO_4$ and PGC were added to 60 ml of distilled water under magnetic stirring to form a homogeneous distribution of the precursor solution. After stirring for 30 minutes, 20 mL of ethanol was added dropwise and the suspension was stirred for 12 h at room temperature to allow slow growth of MnO_2 nanoparticles on the carbon. The obtained composite particles were then filtered and washed repeatedly with enough quantities of DI water until the pH reached 7. The final product abbreviated as MnO_2-PGC was dried at 353 K overnight and stored for further use. Besides, pure MnO_2 particles were also prepared using a similar approach, but in the absence of PGC. The synthesized samples were used as adsorbents directly for all the adsorption experiments performed in this study. Fig. S1 in supplementary section illustrates the experimental procedure used in this study for the synthesis of pure and composite adsorbents based on wet chemical deposition technique

2.3. Material Characterization

The surface morphology and microstructure of the adsorbents before and after sulfide adsorption were analyzed using FEG Quanta 250 scanning electron microscopy (SEM) and FEI Tecnai G20 transmission electron microscopy (TEM). Prior to the SEM analysis, adsorbent

particles were sputter-coated with a conductive layer of gold-palladium (Au/Pd, 3 nm thickness). The zeta potential of the adsorbent samples was measured using Zeta PALS instrument (Brookhaven Instruments Corporation, USA), and elemental analysis was recorded using energy dispersive X-ray spectrometer (Oxford-EDX, UK) fitted to the SEM. Further, the crystalline structure of the adsorbent materials was determined using analytical X'Pert PRO Powder Diffractometer (Cu-Kα radiation 1.5406 A°, 40 kV, 40 mA) in the 2θ range of 5°–80°.

2.4. Adsorption Experiments

Batch adsorption experiments were conducted by adding a certain mass of synthesized adsorbent to about 10 ml of aqueous sulfide solutions with different initial concentrations ranging from 1 mg/L to 200 mg/L in 50 ml stoppered conical flasks. The mass of the adsorbent was varied between 3 and 11 g per 10 ml of sulfide solution to simulate the change in dosage conditions. The flasks were placed in a shaking water bath (Daihan, Korea) maintained at 298 K and subjected to continuous agitation at 140 rpm until equilibrium was attained. It is later shown in the study that the optimum contact time to reach equilibrium for all cases was around 180 min. Sulfide concentrations before and after the adsorption process were measured and analyzed, as demonstrated in section 2.5. All the tests were performed in duplicates. Based on the initial (C_o) and residual equilibrium concentration (C_e), percent removal, and adsorbent uptake capacity at equilibrium (q_e) were calculated, as shown in our previous work (Edathil et al., 2017). Additionally, adsorption experiments were conducted for different contact times (from 1 to 240 min) at fixed process conditions of 200 mg/L initial sulfide concentration, 298 K, and pH 12.

2.5. Measurements of Sulfide

To measure the initial and residual dissolved sulfide concentration in the aqueous solution, 200 µL of pipetted samples were analyzed using LCK 653 sulfide detection kit on UV-vis Spectrophotometer (DR5000, Hach Lange) by the methylene blue method. The sulfide test is based on the reaction of sodium sulfide with N, N-dimethyl-p-phenylenediamine oxalate to directly form methylene blue complex. The intensity of the blue color, as measured by the UV-vis spectrophotometer using Test kit 653 is assumed to be directly proportional to the amount of sulfide present in the original sample (E. Sheppard and H. Hudson, 2002).

3. RESULTS AND DISCUSSION

3.1. Adsorbent Characterization

The morphology and microstructure of the synthesized adsorbents, including δ-MnO_2 and MnO_2-PGC composites, were observed using Scanning Electron Microscopy images, refer Fig. 1(a) and 1(e). In addition, EDX data presented in Fig. 1(b) and 1(f) serve to determine the elemental composition of the adsorbents. The surface morphology of δ-MnO_2 exhibited both dense nanosized particles in a size range of 100-200 nm and micro-sized balls. EDX spectra of δ-MnO_2 revealed the presence of both manganese and oxygen with trace quantities of other elements from the coating process. With the addition of PGC, it could be noticed that the porous interconnected microstructure of carbon acts as a basic building block upon which δ-MnO_2 nanoparticles are deposited. The EDX spectra of MnO_2-PGC revealed the distinct pattern peaks of magnesium in addition to the peaks of carbon, oxygen, and calcium which are the major constituent elements present in the PGC. The coexistence of all these elements in the obtained EDX results clearly proves the formation of MnO_2-PGC composites. The SEM images of spent (sulfide adsorbed) δ-MnO_2 and MnO_2-PGC composite has been illustrated in Fig. 1(c) and 1(g) with the corresponding EDX results in Fig. 1(d) and 1(h). It could be noted that following the

adsorption process using δ-MnO_2, the adsorbent surface underwent structural changes and predominantly displayed small aggregates of elemental sulfur and sulfate nanoparticles, suggesting successful adsorption/oxidation of sulfide. The presence of Na and S in the EDX results, see Fig. 1(d) further confirms that sulfide has been oxidized to sodium sulfate and/or elemental sulfur. The composite adsorbent also showed the presence of irregular particles with an aggregated surface on both the carbon walls as well as on the surface of MnO_2 nanoparticles. Furthermore, EDX spectra of sulfide-adsorbed MnO_2-PGC shows a characteristic peak for sulfur particles along with carbon, oxygen, and calcium. These results further confirm the successful adsorptive oxidation of sulfide on the surface of the adsorbent to calcium sulfate and/or elemental sulfur.

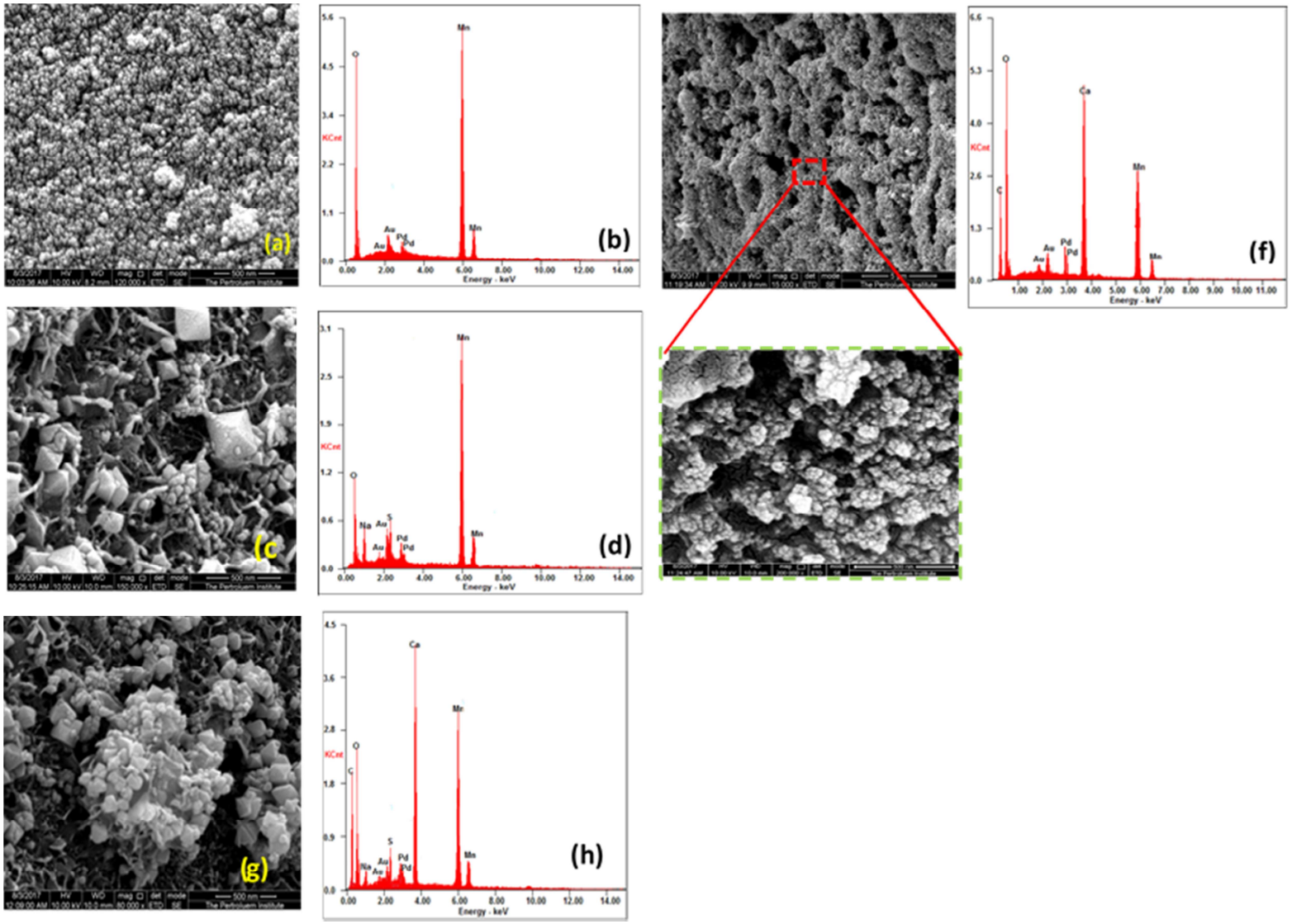

Fig. 1: Scanning Electron Microscopy (SEM) and EDX results of nanoparticle composites: (a-b) fresh MnO_2 (c-d) spent MnO_2 (e-f) Fresh -MnO_2-PGC composite (g-h) sulfide adsorbed MnO_2-PGC composite.

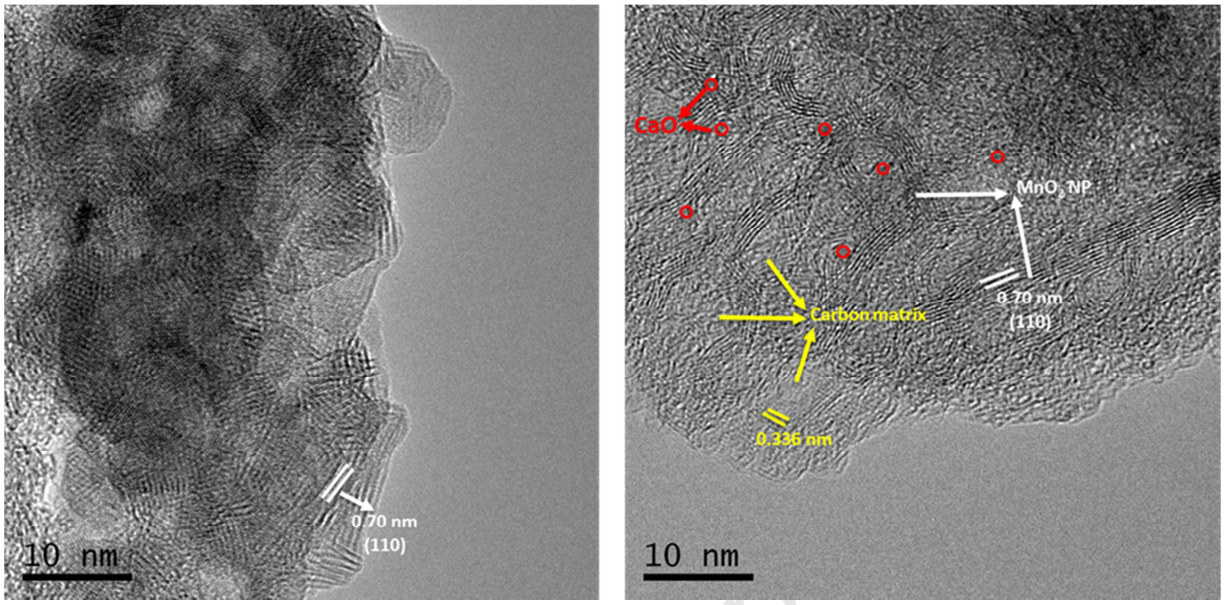

Fig. 2: Transmission Electron Microscopy (TEM) images of synthesized (a) δ-MnO_2 and (b) MnO_2-PGC composite.

To better understand the changes in morphological microstructure induced by in-situ composite synthesis, TEM micrographs of δ-MnO_2 and MnO_2-PGC composite were recorded at higher magnifications and are shown in Fig. 2(a) and 2(b). TEM images of δ-MnO_2 (Fig. 2(a)) revealed the nanoscale architecture of MnO_2 particles with significant agglomeration, which agrees well with the SEM results. The lattice fringe spacing is 0.7 nm corresponding to the (110) plane of δ-MnO_2 (Subramanian et al., 2008). On the other hand, it can be noticed from the TEM image of MnO_2-PGC composite that the MnO_2 nanoparticles are interconnected and uniformly distributed on the surface of the PGC. Along with the lattice fringe of 0.336 nm indexed to (002) plane of graphitic carbon, the composites also showed the lattice fringe spacing corresponding to the (110) plane of δ-MnO_2. Furthermore, the presence of microcrystalline domain of calcium nanoparticles (indicated by the red circle) that are formed by the special 'egg-box' structure of the

188 alginate precursor containing organic calcium salts was observed in the TEM image of the
189 composites (Edathil et al., 2017).
190

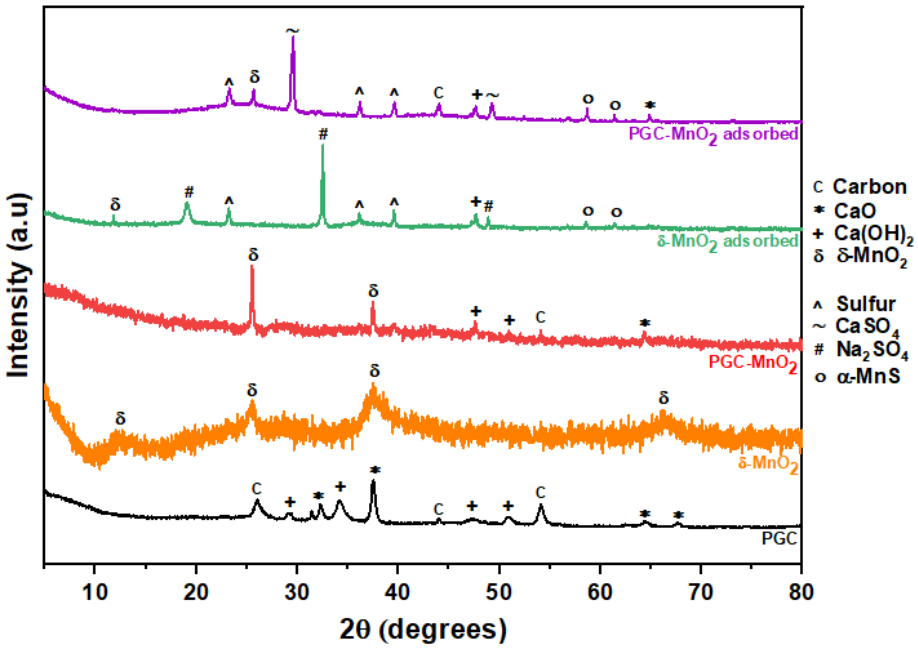

Fig. 3: X-ray diffractograms of various fresh and spent adsorbents.

191 Fig. 3 shows representative X-ray diffractograms of both fresh and spent composite
192 adsorbents in addition to fresh and spent δ-MnO_2 adsorbents and raw PGC. In porous graphitic
193 carbon, the prominent Bragg reflection observed at 26.1°, 44°, and 54° corresponds to the (002),
194 (101) and (004) planes of the graphitic carbon matrix (JCPDS file number 41-1487).
195 Additionally, the diffractogram also showed the presence of calcium oxide and calcium
196 hydroxide particles in the carbonaceous matrix. The diffractogram of δ or Birnessite type MnO_2
197 (JCPDS no. 43-1456) showed characteristic diffraction peaks at 12.8°, 24.8°, 37.6°, and 66.4°
198 attributed to (001), (001), (111) and (311) planes. In the diffractogram of fresh MnO_2-PGC
199 composite, the position of the main diffraction peak of graphitic carbon and δ-MnO_2 was well

retained. On the other hand, XRD of sulfide adsorbed δ-MnO_2, and MnO_2-PGC composite clearly indicated the presence of additional peaks with higher intensity. The oxidation of sulfide components by δ-MnO_2 and MnO_2-PGC to elemental sulfur could be confirmed by the presence of predominant peaks (labeled by ^ in Fig. 3) observed at 23.3°, 36.2° and 39.5° that correspond to the (222) plane of orthorhombic sulfur having S_8 structure (JCPDS 74-1465). Moreover, the XRD of spent δ-MnO_2 showed the presence of additional peaks at 19.1°, 32.5° and 48.9° (labeled by # in Fig. 3) corresponding to the (111), (200) and (300) planes of sodium sulfate (Na_2SO_4). However, the diffractogram of sulfide adsorbed MnO_2-PGC composites showed dominant peaks at 29.5° and 49.3° related to the (202) and (600) planes of $CaSO_4$, indicating the formation of calcium sulfate complex (labeled by ~ in Fig. 3). The presence of additional peaks in spent adsorbents further verifies that oxidation of sulfide ions has occurred.

3.2. Adsorption of Sulfide Ions by Synthesized Adsorbents

3.2.1. Effect of Solution pH

The effect of solution pH on sulfide removal from aqueous solution was investigated under identical conditions (C_0 = 202 mg/L, m = 0.01 g, t = 180 min, T = 298 K) for both MnO_2 and MnO_2-PGC composites. Adsorption experiments were performed at different pH values in the range of 3 to 12, and the corresponding adsorbent removal efficiencies are illustrated in Fig. 4. The data indicates that the adsorption behaviour of both the adsorbents was not affected by the solution pH, and the percent removal was marginally higher for the MnO_2-PGC composite than MnO_2 nanoparticles. In aqueous solutions, sulfides mainly exist in the form of H_2S_{aq}, HS^- and S^{2-} ions. Under strongly acidic conditions with pH <6, sulfides are mainly present in the form of H_2S_{aq} and HS^-, while it contains negligible S^{2-}ions. Whereas at higher pH > 6, the aqueous

223 solution predominantly contains S^{2-} along with HS^- ions, and the concentration of HS^- ions
224 further increase

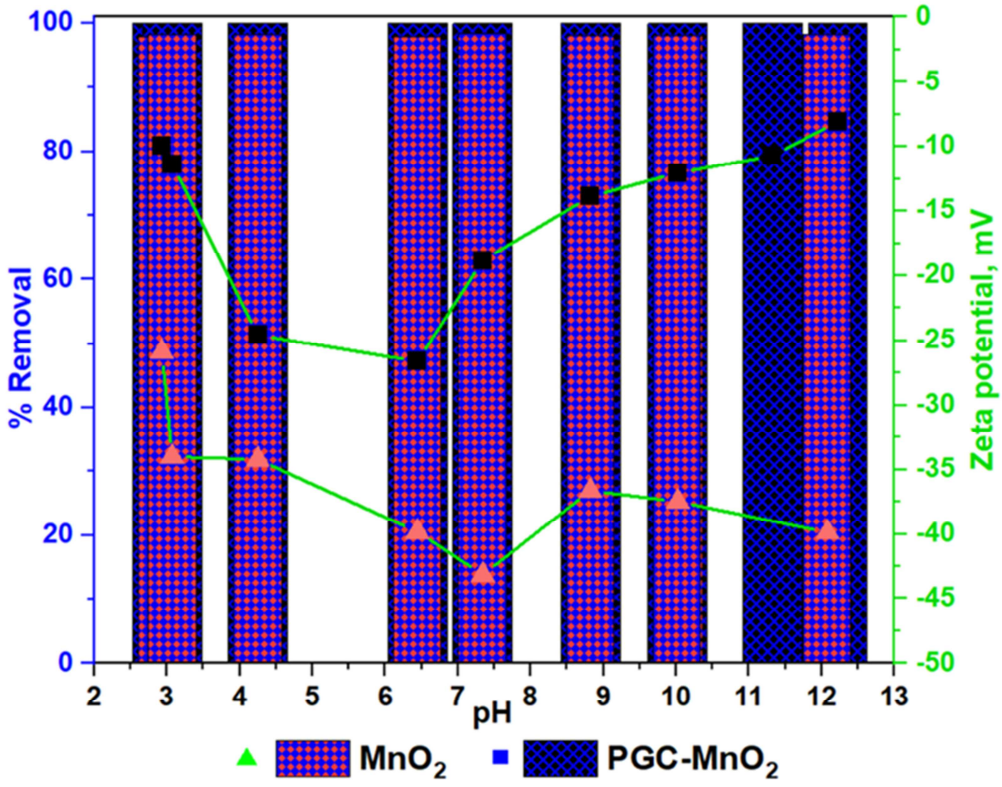

Fig. 4: Effect of pH on sulfide removal using different adsorbents.

225 under strongly alkaline conditions (pH 9 to 12). The obtained pH results clearly indicates that the
226 adsorptive oxidation of sulfide by MnO_2 and MnO_2-PGC was not hindered by adsorption sites as
227 well as the competitive adsorption. Henceforth, the adsorption process of sulfide is found to be
228 less affected by initial solution pH, inferring that the developed composite adsorbent holds the
229 potential to effectively adsorb sulfide from aqueous solution at all pH. Zeta potential
230 measurements were carried out with the aim of understanding (1) the pronounced selective
231 adsorption characteristic exhibited by δ-MnO_2 and MnO_2-PGC for sulfide species, (2) the effect

of surface charge on sulfide adsorption, and (3) the stability of the system. It was interesting to observe that both adsorbents exhibited high surface negative charge at all solution pH. Since the surface charge of the as-prepared adsorbents was negative in the experimental pH range as indicated by the Zeta potential (Fig. 4), most likely chemisorption is caused by an electron transfer reaction with the surface-active sites. The zeta potential of δ-MnO_2 ranging from -25 to -40 mV was caused by the presence of MnO groups on the surface of δ-MnO_2. MnO_2-PGC composite also showed high negative surface charge and may be attributed to the presence of carboxyl and hydroxyl groups obtained from the alginate molecules in addition to the MnO-groups from δ-MnO_2 particles. Even though the absolute values of the zeta potential for both these adsorbents under the investigated pH range (3 to 12) were high (suggesting its good stability in the colloidal state), the composites exhibited slightly higher sulfide removal efficiency. This could be attributed to the better accessibility of the active sites owing to the interconnected porous structure of the carbon. Thus, the active functional groups present on the surface of the developed adsorbents were believed to be less affected by the initial solution pH, thereby contributing to the extraordinary adsorption efficiency showcased all pH conditions. Henceforth, all further adsorption experiments were carried out at the original solution pH of 12.06.

3.2.2. Effect of Ionic Strength

The possible presence of background salts in sulfide containing industrial wastewater tends to form complex metals that might compete with sulfide species for available adsorption sites. The influence of ionic strength on sulfide removal efficiency by the nanocomposite adsorbents was assessed through the addition of NaCl and $CaCl_2$ to the sulfide solution. The

255 concentration of background electrolytes in the sulfide solution was varied from 0 to 1 M.
256 Adsorption studies were conducted in a batch mode at a temperature of 298 K, adsorbent dosage
257 of 1 mg/L, and initial sulfide concentration of 202 mg/L. Adsorption results as shown in Fig S2,
258 showed no significant change in removal efficiency after the addition of background electrolytes
259 to the sulfide solution.

260

261 **3.2.3. Effect of Adsorbent Dose**

262 The effect of adsorbent dose on sulfide adsorption by MnO_2 and MnO_2-PGC
263 nanocomposite has been presented in Fig. 5. Experiments were performed at the following
264 conditions: initial sulfide concentration of 202 mg/L, 180 min, 298 K, and a solution pH of
265 12.06. Adsorbent mass was varied between 2.5 and 20 mg that corresponds to a dosage of 0.25
266 g/L to 2 g/L. It can be noticed that the removal efficiency increases with adsorbent dosage till ca.
267 1 g/L, at which point the efficiency reaches a maximum. The initial increase in removal
268 efficiency is a direct result of increased contact surface area, more specifically the active sites
269 offered by the adsorbent. However, with further increasing the adsorbent dosage, the effective
270 surface area is significantly affected, resulting from overlapping or aggregation of sulfide
271 molecules near the adsorption site (Ahluwalia and Goyal, 2007). As a result, all the active sites
272 are not fully utilized, thereby leading to a decrease in the adsorption capacity, as evidenced in the
273 SEM images, refer Fig. 1e.

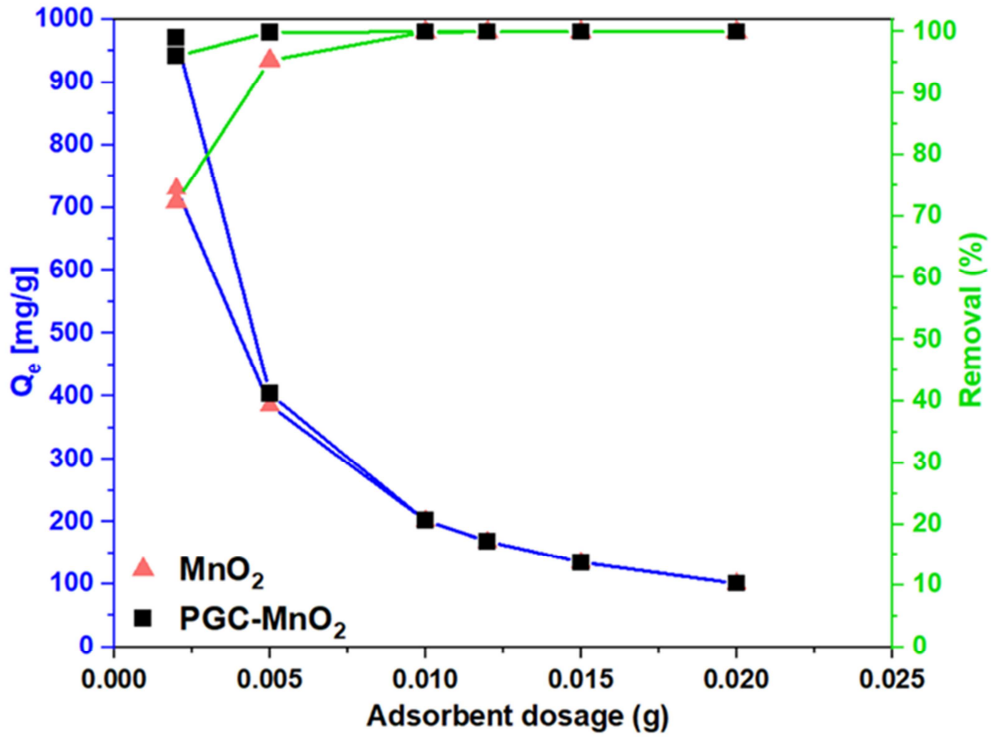

Fig. 5: Effect of adsorbent mass on sulfide removal using different adsorbents.

3.2.4. Effect of Initial Sulfide Ion Concentration

The amount of sulfide ions adsorbed is proportionally controlled by the initial concentration of sulfide ions in the solution making it a crucial parameter for sensitivity analysis. All the parameters adsorbent dosage (1 g/L), agitation time (180 min), temperature (298 K), and pH (12.06) except initial concentration were kept constant. The effect of initial ion concentration (varying from 0 to 600 mg/L) on equilibrium adsorption capacity and removal efficiency of sulfide ions on the adsorbent is shown in Fig. 6. As shown, sulfide removal efficiency for the MnO_2 nanoparticle sample exhibited a gradually decreasing trend till 300 mg/L, beyond which a sharp decrease could be noticed. A similar trend could be observed for the nanocomposite sample, however, less pronounced.

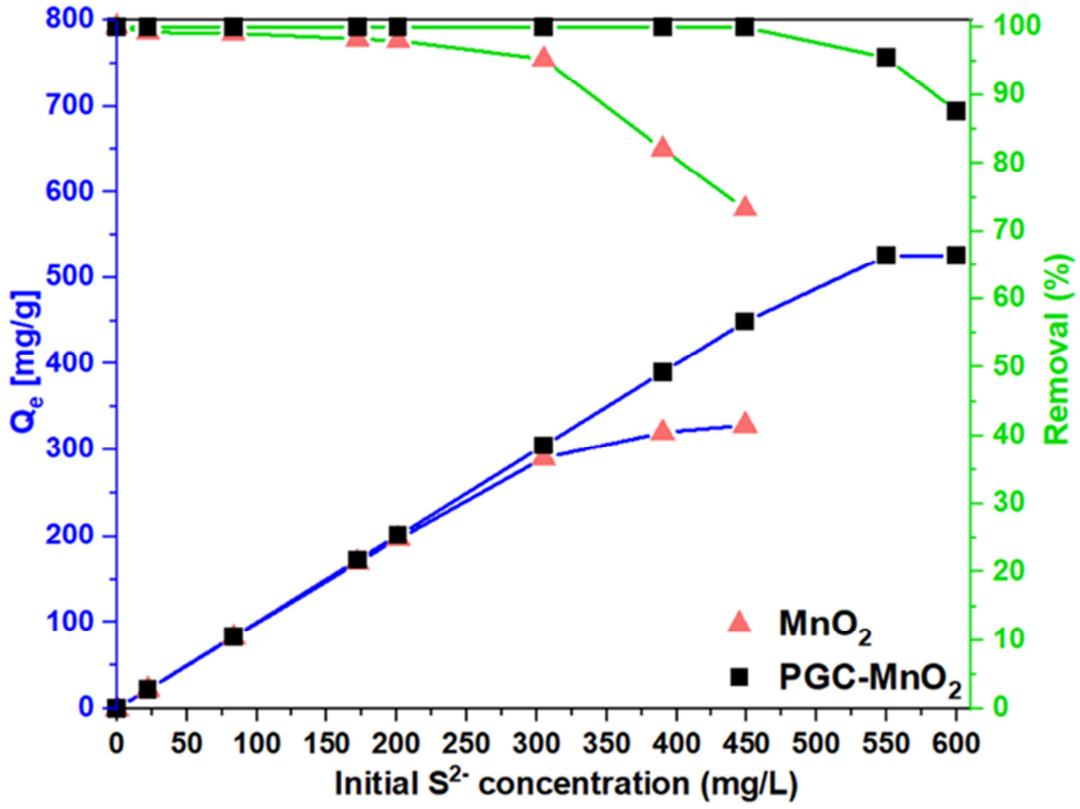

Fig. 6: Effect of initial sulfide solution concentration on sulfide removal using different adsorbents.

Contrastingly, with an increase in initial sulfide ion concentration, an increase in adsorption capacity for both samples could be noticed. The steady increase could be attributed to the increased local concentration gradient of sulfide ions between the solid and aqueous phase that subsequently results in higher sulfide ion fixation at the surface area and maximum utilization of the available active sites (Barka et al., 2013). However, when the active sites are saturated with sulfide ions, the equilibrium adsorption capacity remains constant. The maximum adsorption capacity is significantly higher for the composite (505 mg/g) in comparison to the

291 MnO_2 nanoparticle (ca. 310 mg/g), thereby indicating the positive impact of introducing δ-MnO_2
292 particle into the interconnected morphology of the porous graphitic carbon.

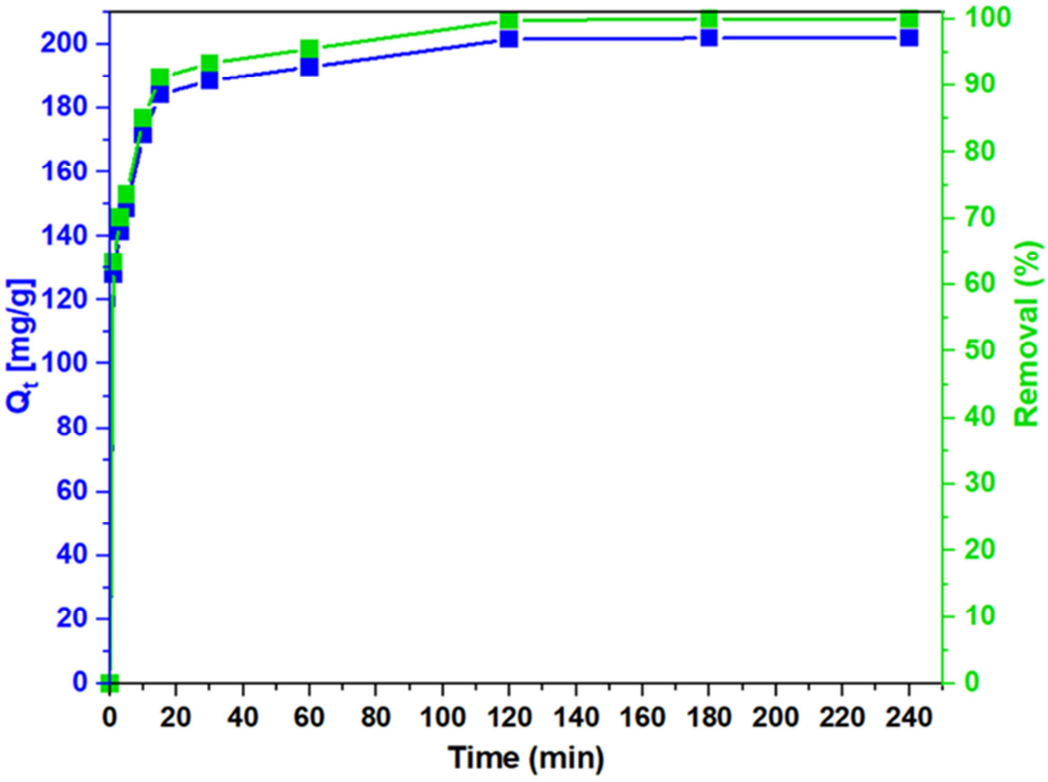

Fig. 7: Effect of contact time on removal efficiency and uptake capacity.

293 **3.2.5. Effect of Contact Time**

294 In order to determine the time required for achieving adsorption equilibrium, it is
295 significant to assess the influence of agitation time on adsorption capacity and efficiency. Fig. 7
296 depicts the effect of agitation time on the adsorption of sulfide ions over MnO_2-PGC adsorbent at
297 fixed conditions of initial concentration (202 mg/L), adsorbent dosage (1 g/L), temperature (298
298 K), and pH (12.06). At the early stages of adsorption (t<20 min), a rapid increase in removal
299 efficiency and adsorption capacity could be observed. Beyond 20 minutes, the effect gradually

diminished until it displayed no significant increase beyond 120 minutes. The residual concentration at 180 min was found to be approximately about 0.8% of that obtained after 240 min. Accordingly, a quasi-equilibrium condition was assumed to have been reached at 180 min, and henceforth all succeeding batch experiments were conducted for 180 min. The pronounced increased rate at early stages could be attributed to the availability of abundant vacant active sites on the adsorbent. As adsorption proceeds, sulfide ions gradually occupy the vacant sites at a much slower rate until a point of saturation. The decreased sorption rate is possibly due to the larger diffusion path lengths deeper into the adsorbent pores where the sulfide ions encounter higher mass transfer resistance. No significant change in sulfide concentration was observed after 180 min as all sites have been occupied, and equilibrium is established.

3.3. Adsorption Kinetic Studies

To evaluate the adsorption rate and elucidate the reaction mechanism of sulfide ions on MnO_2-PGC composites, experimental data were analyzed using the frequently employed kinetic models, including pseudo-first-order (PFO), pseudo-second-order reaction (PSO), and intraparticle diffusion (IPD) models. In a well-agitated batch system, the resistance offered by the film is negligible in comparison to the adsorbent internal microstructure (surface and pore). The diffusion mass transfer can be captured by an apparent diffusion coefficient that ensembles the different steps involved in the intraparticle diffusion process. The behavior of intraparticle diffusion could be explained by the Weber & Morris intra-particle diffusion model (IPD) as: (Dil et al., 2016; Nekouei et al., 2015; Weber and Morris, 1963)

$$q_t = k_i\, t^{0.5} + C \quad (1)$$

where k_i is the intra-particle diffusion rate constant (mg/g. $min^{0.5}$) and C is the empirical constant (mg/g). The value of C depends on the film boundary layer thickness wherein a larger value of C represents a significant effect of the boundary layer on adsorbate diffusion (Kannan and Sundaram, 2001). Typically, the rate-controlling step is deduced by analyzing the linear relationship between q_t and $t^{0.5}$, as shown in supplementary file Fig. S3. It can be noticed that the experimental data exhibits three different linear parts (I, II, III), each possibly indicating different stages of intra-particle diffusion. The first part refers to the least-resistive external surface adsorption or macro-pore diffusion, the second part to the relatively less-accessible mesopores, and the third part to micropore diffusion (Cheng et al., 2013). It is evident that the linear part of the diffusion curve (step I) does not pass through the origin, and therefore the diffusion process might not be solely controlled by any specific stage but is probably influenced by multiple steps. The corresponding rate constants and intercept for the three parts are denoted as k_{i1}, C_1, k_{i2}, and k_{i3}, and are summarized in Table 1. It can be noted that the rate constants gradually decrease from 16.72 mg/g.$min^{0.5}$ (step 1) to 3.94 (step II) to 0.09 (step III), strongly indicating increasing diffusion resistance with the progress of the adsorption process. Stage I is predominant when there are numerous vacant sites in the adsorbent particle during the initial stages. However, during stage 2, most of the active sites on the surface are saturated, and hence intra-particle diffusion is limited by the interior mesopores. Finally, at the last step, the sulfide ions diffuse towards micropores and establish equilibrium between the solid and dissolved phases. Moreover, the increasing value of intercept C indicates the deviation from the dominating rate-controlling mechanism as a result of the increasing boundary layer thickness.

Kinetic data analysis using pseudo-first and second-order reaction models is frequently employed to determine how fast adsorption equilibrium would be achieved. For the PFO reaction

model, adsorption rate constant (k_f) was determined by plotting $\ln(q_e - q_t)$ against t for sulfide ion adsorption on MnO_2-PGC composite at an initial concentration of 202 mg/L and 298 K. Values of equilibrium loading (q_e) and second-order rate constant (k_s) for the PSO model was obtained from a linear plot of t/q_t versus t, refer to supplementary file Fig. S4. Model parameters, including rate constants and equilibrium loading, were obtained through linear regression, and the accuracy of the fit was evaluated from the regression coefficient (R^2). Further, in order to assess the error propagated through linearization, the constants were also evaluated using non-linear forms of the model equations and compared with the results from linear forms. A summary of model equations, along with the regressed parameters from different models, have been compiled in Table 1. It could be noticed that both PFO and PSO reaction models predict experimental data reasonably well, as evidenced by the high values of the regression coefficient. Despite the good fit of the PFO linear model, the values of both constants, namely rate constant and equilibrium capacity, are vastly different from the PFO non-linear and PSO model estimates. It should be remembered that the PFO model is applicable only during initial adsorption stages and high adsorbate solution concentration (Wang and Guo, 2020), and thus employing it for larger time frames would induce significant error. The low value of equilibrium adsorbent loading estimated by the PFO linear model could be a direct consequence of extending the model for a wider time step. The q_e values estimated by the PSO linear and non-linear models are in good agreement with the experimentally calculated equilibrium loading values ($q_{e,exp}$).

Table 1: Summary of kinetic model equations and parameters of MnO_2-PGC composite

Model		Equation	Rate constants	q_e (mg/g)		R^2
				$q_{e,\ exp}$	$q_{e,\ cal}$	
PFO	Linear	$\ln(1-(q_t/q_e)) = -k_f t$	k_f = 0.04 ± 0.0018	201.9	56.4 ± 0.9	0.954
	Non-linear	$q_t = q_e(1-e^{-k_f t})$	k_f = 0.86 ± 0.02		184.9± 2.1	0.903
PSO	Linear	$t/q_t = t/q_e + (1/k_s q_e^2)$	k_s = 0.0028±0.0005	201.9	204.1±0.6	0.999
	Non-linear	$q_t = (k_s q_e^2)\ t/(1+k_s q_e t)$	k_s = 0.0065±0.0009		194.7±1.1	0.967
IPD	--	$q_t = k_i t^{(1/2)} + C$	k_{i1} = 16.72±1.2 C_1 = 111.74±2.1	201.9	---	0.99
			k_{i2} = 3.94±1.5			0.77
			k_{i3} = 0.09±0.05			0.79

3.4. Adsorption Isotherms

The experimental data of adsorption isotherms were analysed using three different models, namely Langmuir, Freundlich, and Temkin. The standard mathematical equations describing the models could be found widely in literature, and hence is not presented in this work. Isotherm parameters were estimated by linear regression analysis and are listed in Table S1 along with the corresponding model equations. As shown, the value of the regression coefficient for the Langmuir model equation is 0.99 for both MnO_2 and composite samples. It is an implication that sulfide ion adsorption on both samples follows a monolayer adsorption process with no interaction between the adsorbed molecules. MnO_2-PGC Comparing the value of Langmuir adsorption constant (k_L) between MnO_2 and composite sample, it can be inferred that the affinity of sulfide ion adsorption on MnO_2 is higher than that of MnO_2-PGC composite. However, due to increased surface area, the PGC composite possesses significantly higher adsorption capacity than MnO_2 nanoparticle. The applicability of Freundlich isotherm for sulfide adsorption on MnO_2 and PGC composite was also tested and validated with isotherm experimental data. The solution concentration influence coefficient (1/n) value of 0.05 for MnO_2 sample strongly indicates favourable adsorption. However, the linear regression coefficient for the MnO_2-PGC composite sample was 0.69, which is significantly smaller than that of the Langmuir model. Similarly, the regression coefficient for the Temkin adsorption model is far from unity indicating a non-linear relationship between ln q_e and ln C_e. Therefore, sulfide ion adsorption on MnO_2-PGC composite follows monolayer adsorption, and thus, Langmuir adsorption isotherm is more suitable for modeling the equilibrium process. Based on the results, the maximum sulfide adsorption capacity on MnO_2-PGC composite was estimated to be 526.3

374 mg/g. Compared with other sulfide adsorbents presented in literature, it can be seen from Table 2
375 that MnO_2-PGC exhibited superior adsorption capacity.

Table 2: Comparison of sulfide adsorption capacities for different adsorbents

Adsorbent	Initial Concentration (ppm)	Adsorption capacity (mg/g)	Reference
Granular ferric hydroxide (GFH)	19.8 ± 0.6	29.1 ± 0.6	(Sun et al., 2014)
Alg/Iron Oxide-NP	64.3	136.9	(Pal et al., 2018)
Activated Carbon (AC) - 500˚C	0-1000	58.8	(Hariz and Monser, 2014)
PGC	45	149.25	(Edathil et al., 2017)
GSH Composites	202-450	370.4	(Achazhiyath Edathil et al., 2019)
CeO_2-NiAl-LDHs coated activated carbon	0.1 M	181.15	(Achazhiyath Edathil et al., 2019)
MnO_2 nanoparticle	0-450	303.03	This work
MnO_2-PGC	0-600	526.32	This work

376 **3.5. Reaction Mechanism**

377 The MnO_2-PGC composite was employed for sulfide removal in order to exploit the
378 advantages of the oxidative nature of MnO_2 and the surface functionality of PGC offered by
379 oxygen functional groups. To further understand the mechanism involved in
380 adsorption/oxidation, it is of great importance to understand the elementary reaction step
381 involved in the dissolution of crystalline hydrate of Na_2S in water. In aqueous alkaline solution,
382 dissolution of Na_2S solution yields sulfides $[S_{aq}^{2-}]$, bisulfides $[HS_{aq}^{-}]$ and aqueous H_2S $[H_2S_{aq}]$

383 (Linkous et al., 2004). Thus, the interaction of the dissolved sulfur species with oxygen
384 functional groups present on the PGC and the MnO_2 nanoparticles results in the distribution of
385 sulfides oxidation products over the composite adsorbent surface The $C(O^*)_{(ads)}$ species which is
386 the oxygen-containing active sorption site and/or radical of the form C (O*) on the carbon
387 surface, are believed to be responsible for the successful adsorptive oxidation of sulfide to
388 different species such as elemental sulfur and calcium sulfate. When aqueous hydrogen sulfide
389 ions contact the graphitic carbon surface, it undergoes oxidative decomposition to produce sulfur
390 atoms. Sulfur atoms react in a substitution reaction with the C(O) surface complex and in an
391 addition reaction with radical C* to form C-S complexes and continue until the formation of
392 elemental sulfur chains (S_8). The possible redox reaction involved in the formation of elemental
393 sulfur by PGC is illustrated as below:
394

$$HS^- + C(O^*)_{(ads)} \rightarrow S_{(ads)} + OH^-$$

$$H_2S_{(ads)} + C(O^*)_{(ads)} \rightarrow \frac{1}{8} {S_8}^0 + H_2O + C^*$$

395
396 In aqueous medium, bisulfides (HS^-) reacts with the oxygen functional groups to form sulfur
397 oxides, $SO_{2(ads)}$ and $SO_{3(ads)}$ and is as evidenced in the literature (Brazhnyk et al., 2007; Lemos
398 et al., 2012). These sulfur oxides further react with water resulting in the formation of sulfate
399 ions (SO_4^{2-}) that continues to react with calcium metal ions present in the PGC matrix to form
400 calcium sulfates. XRD further confirms the presence of $CaSO_4$.
401

$$HS^- + 3\ C(O^*)_{(ads)} \rightarrow SO_{2(ads)} + OH^-$$

402 $$SO_{2(ads)} + C(O^*)_{(ads)} \rightarrow SO_{3(ads)} + C^*$$

403 $$SO_{3(ads)} + H_2O \rightarrow 2H^+ + {SO_4}^{2-}$$

$$SO_4^{2-} + Ca^{2+} \rightarrow CaSO_4 0.5H_2O$$

404 The production of elemental sulfur [S_8^0] by MnO_2 proceeds through a series of surface complex
405 formation initiated by the adsorption of HS^- onto the manganese oxide surface followed by
406 oxidation as illustrated below:

407

$$S^{2-} + 2MnO_{2(ads)} + 2H_2O \rightarrow + 2MnOOH + S^0 + 2OH^-$$

408

409 With MnOOH as catalyst,

410

$$S^{2-} + 2H_2O + O_2 \rightarrow 2S^0 + 4OH^-$$

$$MnO_{2(ads)} + HS^- \rightarrow {Mn^{2+}}_{(ads)} + 2H_2O + \frac{1}{8}\,{S_8}^0$$

$${Mn^{2+}}_{(ads)} + 2H_2O \leftrightarrow Mn(OH)_{2(ads)} + H^+$$

411 $$2Mn(OH)_{2(ads)} + 2O_2 \leftrightarrow 2MnO(OH)_{2(ads)}$$

412 $$2MnO(OH)_{2(ads)} \leftrightarrow {MnO_{2(ads)}}^* + H_2O$$

413

414 The adsorbed HS^- ions also participate in redox reactions to form an intermediate metal
415 surface complex MnS that could undergo two different competitive reaction pathways to form
416 elemental sulfur and sulfates through the formation of zero-valent sulfur intermediate (Herszage
417 and dos Santos Afonso, 2003).

418

$$MnO_{2(ads)} + H_2O \rightarrow \quad MnOH^{2+}{}_{(ads)}$$

$$MnOH^{2+}{}_{(ads)} + HS^- \rightarrow MnS_{(ads)} + H_2O$$

$$MnS_{(ads)} + H_2O \rightarrow \quad MnOH_{2(ads)} + S^0$$

$$MnOH_{2(ads)} \rightarrow \quad MnOH^{2+}{}_{(ads)}{}^{*} + Mn^{2+}{}_{(aq)}$$

$$S + HS^- \rightarrow HS_2^-$$

$$HS_2^- + 7S \rightarrow S_8 + HS^-$$

$$MnOH_{2(ads)} + MnS_{(ads)} + \quad MnOH^{2+}{}_{(ads)} \rightarrow SO_4{}^{2-} + 3MnOH_{2(ads)}$$

$$SO_4{}^{2-} + Na^{2+}{}_{(aq)} \rightarrow NaSO_{4(aq)}$$

Oxidation of S_{aq}^{2-}, HS_{aq}^- and H_2S_{aq}species by MnO_2-PGC composites was experimentally verified by the presence of sulfate in the form of calcium sulfate and elemental sulfur from XRD analysis. Results from EDX also confirm the participation of MnO_2 in the oxidizing reaction resulting in the formation of various sulfur species. In addition, with the deposition of MnO_2 on PGC, the maximum adsorption capacity was significantly enhanced when compared to bare PGC, which was reported to be 149.2 mg/g (Edathil et al., 2017). The high values of solid adsorbent loading and negligible liquid phase equilibrium concentrations at low sulfide initial concentration conditions are an indication of the formation of metal complexes, including calcium sulfate wherein the rate of adsorption is very high relative to the rate of desorption. The results obtained from XRD and EDX well support the combined effect of PGC and MnO_2 on oxidation of sulfide molecules. However, techniques for desorbing the sulfide contaminants from the adsorbent needs to be investigated before recovery and reuse of spent adsorbent could be envisaged.

CONCLUSION

The feasibility of employing the MnO_2-PGC composite adsorbent for the removal of hazardous sulfide components from aqueous systems was investigated through batch adsorption studies at different process conditions. MnO_2-PGC nanocomposite adsorbents were synthesized via the in-situ chemical wet deposition method using PGC derived from calcium alginate as carbon precursor. The synthesized fresh composite and spent adsorbent were examined using TEM, SEM, EDX and XRD and revealed that the surface modification of PGC by MnO_2 nanoparticles helped in drastically enhancing the oxidative capability of bare carbon. It was found that the removal efficiency of the adsorbent was not affected by the solution pH; however, it was dependent on the initial sulfide ion concentration. Kinetic studies inferred that adsorption of sulfide ions by MnO_2-PGC composite was well-described by pseudo-second-order kinetic model, confirming that chemisorption controlled the overall rate of sulfide sorption. Experimental isotherm data confirmed the suitability of the Langmuir model for describing the equilibrium conditions, and the maximum adsorption capacity was estimated to be 526.3 mg/g, significantly higher than that of PGC. Results confirmed that the high adsorption capacity could be attributed to the reactivity of bounded MnO_2, and oxygen atoms present on the active sites of PGC with interconnected morphology that oxidized sulfide contaminants to sulfates and elemental sulfur. In summary, the excellent adsorptive characteristics demonstrate that the MnO_2-PGC composites can serve as an adsorbent material to remove hazardous sulfide contaminants from aqueous solution.

Conflict of Interest

There are no conflicts of interest to declare.

Acknowledgment

The authors would like to gratefully acknowledge the financial support kindly provided by Khalifa University under Grant No. LTR14013.

REFERENCES

Achazhiyath Edathil, A., Hisham Zain, J., Abu Haija, M., Banat, F., 2019. Scalable synthesis of an environmentally benign graphene–sand based organic–inorganic hybrid for sulfide removal from aqueous solution: an insight into the mechanism. New J. Chem. 43, 3500–3512. https://doi.org/10.1039/C8NJ05301D

Ahluwalia, S.S., Goyal, D., 2007. Microbial and plant derived biomass for removal of heavy metals from wastewater. Bioresour. Technol. 98, 2243–2257. https://doi.org/10.1016/J.BIORTECH.2005.12.006

Amiri, A., Baghayeri, M., Hamidi, E., 2018. Poly(pyrrole-co-aniline)@graphene oxide/Fe3O4 sorbent for the extraction and preconcentration of polycyclic aromatic hydrocarbons from water samples. New J. Chem. 42, 16744–16751. https://doi.org/10.1039/C8NJ03936D

Artiga, P., Ficara, E., Malpei, F., Garrido, J.M., Méndez, R., 2005. Treatment of two industrial wastewaters in a submerged membrane bioreactor. Desalination 179, 161–169. https://doi.org/https://doi.org/10.1016/j.desal.2004.11.064

Barka, N., Abdennouri, M., El Makhfouk, M., Qourzal, S., 2013. Biosorption characteristics of cadmium and lead onto eco-friendly dried cactus (Opuntia ficus indica) cladodes. J. Environ. Chem. Eng. 1, 144–149. https://doi.org/10.1016/J.JECE.2013.04.008

Bono, A., Ramlan, N.A., Anisuzzaman, S.M., Chu, C.M., Farm, Y.Y., 2016. Adsorption isotherm of non-azeotropic solution onto porous adsorbents. IOP Conf. Ser. Earth Environ. Sci. 36, 012021. https://doi.org/10.1088/1755-1315/36/1/012021

Brazhnyk, D. V., Zaitsev, Y.P., Bacherikova, I. V., Zazhigalov, V.A., Stoch, J., Kowal, A., 2007. Oxidation of H2S on activated carbon KAU and influence of the surface state. Appl. Catal. B Environ. 70, 557–566. https://doi.org/10.1016/J.APCATB.2005.12.028

Burakov, A.E., Galunin, E. V, Burakova, I. V, Kucherova, A.E., Agarwal, S., Tkachev, A.G., Gupta, V.K., 2018. Adsorption of heavy metals on conventional and nanostructured materials for wastewater treatment purposes: A review. Ecotoxicol. Environ. Saf. 148, 702–712. https://doi.org/https://doi.org/10.1016/j.ecoenv.2017.11.034

Cadena, F., Peters, R.W., 1988. Evaluation of chemical oxidizers for hydrogen sulfide control. J. Water Pollut. Control Fed. 60, 1259–1263.

Chai, S.-H., Howe, J.Y., Wang, X., Kidder, M., Schwartz, V., Golden, M.L., Overbury, S.H., Dai, S., Jiang, D., 2012. Graphitic mesoporous carbon as a support of promoted Rh catalysts for hydrogenation of carbon monoxide to ethanol. Carbon 50, 1574–1582. https://doi.org/10.1016/J.CARBON.2011.11.036

Chen, Q., Yao, Y., Li, X., Lu, J., Zhou, J., Huang, Z., 2018. Comparison of heavy metal removals from aqueous solutions by chemical precipitation and characteristics of precipitates. J. Water Process Eng. 26, 289–300. https://doi.org/https://doi.org/10.1016/j.jwpe.2018.11.003

Cheng, C. (Sage), Deng, J., Lei, B., He, A., Zhang, X., Ma, L., Li, S., Zhao, C., 2013. Toward 3D graphene oxide gels based adsorbents for high-efficient water treatment via the promotion of biopolymers. J. Hazard. Mater. 263, 467–478. https://doi.org/10.1016/J.JHAZMAT.2013.09.065

Dil, E.A., Ghaedi, M., Ghaedi, A.M., Asfaram, A., Goudarzi, A., Hajati, S., Soylak, M., Agarwal, S., Gupta, V.K., 2016. Modeling of quaternary dyes adsorption onto ZnO–NR–AC artificial neural network: Analysis by derivative spectrophotometry. J. Ind. Eng. Chem. 34, 186–197. https://doi.org/https://doi.org/10.1016/j.jiec.2015.11.010

Dohnalek, D.A., FitzPatrick, J.A., 1983. The chemistry of reduced sulfur species and their removal from groundwater supplies. J. Am. Water Work. Assoc. 75, 298–308. https://doi.org/10.1002/j.1551-8833.1983.tb05142.x

E. Sheppard, S., H. Hudson, J., 2002. Determination of labile sulfur in gelatin and proteins. Ind. Eng. Chem. Anal. Ed. 2, 73–75. https://doi.org/10.1021/ac50069a030

Edathil, A.A., Pal, P., Banat, F., 2017. Alginate derived porous graphitic carbon for highly efficient remediation of sulfide from wastewater. J. Environ. Chem. Eng. 5, 1998–2009. https://doi.org/https://doi.org/10.1016/j.jece.2017.04.009

Firer, D., Friedler, E., Lahav, O., 2008. Control of sulfide in sewer systems by dosage of iron salts: Comparison between theoretical and experimental results, and practical implications. Sci. Total Environ. 392, 145–156. https://doi.org/https://doi.org/10.1016/j.scitotenv.2007.11.008

Gokulakrishnan, N., Kania, N., Léger, B., Lancelot, C., Grosso, D., Monflier, E., Ponchel, A., 2011. An ordered hydrophobic P6mm mesoporous carbon with graphitic pore walls and its application in aqueous catalysis. Carbon 49, 1290–1298. https://doi.org/10.1016/J.CARBON.2010.11.048

Gupta, V.K., Nayak, A., Agarwal, S., 2015. Bioadsorbents for remediation of heavy metals: Current status and their future prospects. Environ. Eng. Res. 20, 1–18. https://doi.org/10.4491/eer.2015.018

Gupta, V.K., Saleh, T.A., 2013. Sorption of pollutants by porous carbon, carbon nanotubes and fullerene- An overview. Environ. Sci. Pollut. Res. 20, 2828–2843. https://doi.org/10.1007/s11356-013-1524-1

Hariz, I. Ben, Monser, L., 2014. Sulfide removal from petroleum refinery wastewater by adsorption on chemically modified activated carbon. Int. Water Technol. J. 4, 264–267.

Heideman, E., Aoki, H., Segala, E., Segala, J., 1984. Oxidation des sulfures dans la recirculation des liqueres depelanage. Rev. Techn. Ind. Cuir 76, 221.

Herszage, J., dos Santos Afonso, M., 2003. Mechanism of Hydrogen Sulfide Oxidation by Manganese(IV) Oxide in Aqueous Solutions. Langmuir 19, 9684–9692. https://doi.org/10.1021/la034016p

Kannan, N., Sundaram, M.M., 2001. Kinetics and mechanism of removal of methylene blue by adsorption on various carbons—a comparative study. Dye. Pigment. 51, 25–40. https://doi.org/10.1016/S0143-7208(01)00056-0

Kociolek-Balawejder, E., Wilk, L.J., 2011. Sulfides in industrial systems. Technical and environmental problems [in Polish]. Przem. Chem. 90, 825–830.

Komanowsky, M., Senske, G.E., Aceto, N.C., Sin-Namon, H.I., 1984. Recovery of sulfide from tannery effluents. J. Am. Leather Chem. Assoc. 79, 252–270.

La, D.D., Thi, H.P.N., Nguyen, T.A., Bhosale, S. V, 2017. Effective removal of Pb(ii) using a graphene@ternary oxides composite as an adsorbent in aqueous media. New J. Chem. 41, 14627–14634. https://doi.org/10.1039/C7NJ03064A

Lemos, B.R.S., Teixeira, I.F., de Mesquita, J.P., Ribeiro, R.R., Donnici, C.L., Lago, R.M., 2012. Use of modified activated carbon for the oxidation of aqueous sulfide. Carbon 50, 1386–1393. https://doi.org/10.1016/J.CARBON.2011.11.011

Li, Y., Zhao, R., Chao, S., Sun, B., Zhang, N., Qiu, J., Wang, C., Li, X., 2017. A flexible magnesium silicate coated electrospun fiber adsorbent for high-efficiency removal of a toxic cationic herbicide. New J. Chem. 41, 15601–15611. https://doi.org/10.1039/C7NJ03168H

Linkous, C.A., Huang, C., Fowler, J.R., 2004. UV photochemical oxidation of aqueous sodium sulfide to produce hydrogen and sulfur. J. Photochem. Photobiol. A Chem. 168, 153–160. https://doi.org/10.1016/J.JPHOTOCHEM.2004.03.028

Lu, L., Yu, W., Wang, Y., Zhang, K., Zhu, X., Zhang, Y., Wu, Y., Ullah, H., Xiao, X., Chen, B., 2020. Application of biochar-based materials in environmental remediation: from multi-level structures to specific devices. Biochar 2, 1–31. https://doi.org/10.1007/s42773-020-00041-7

Marais, T.S., Huddy, R.J., Harrison, S.T.L., Hille, R.P. van, 2020. Demonstration of simultaneous biological sulphate reduction and partial sulphide oxidation in a hybrid linear flow channel reactor. J. Water Process Eng. 34, 101143. https://doi.org/https://doi.org/10.1016/j.jwpe.2020.101143

Mestrinelli, F., Pozzi, E., Sakamoto, I.K., Foresti, E., 2016. Isolation and characterization of a microorganism involved in sulfide-oxidizing autotrophic denitrification in a vertical fixed-bed reactor. J. Water Process Eng. 11, 138–142. https://doi.org/https://doi.org/10.1016/j.jwpe.2016.04.003

Mondal, M.K., Roy, D., Chowdhury, P., 2018. Designed functionalization of reduced graphene oxide for sorption of Cr(vi) over a wide pH range: a theoretical and experimental perspective. New J. Chem. 42, 16960–16971. https://doi.org/10.1039/C8NJ03794A

572 Nekouei, F., Nekouei, S., Tyagi, I., Gupta, V.K., 2015. Kinetic, thermodynamic and isotherm
573 studies for acid blue 129 removal from liquids using copper oxide nanoparticle-modified
574 activated carbon as a novel adsorbent. J. Mol. Liq. 201, 124–133.
575 https://doi.org/https://doi.org/10.1016/j.molliq.2014.09.027

576 Pal, P., Edathil, A.A., Chaurasia, L., Rambabu, K., Banat, F., 2018. Removal of sulfide from
577 aqueous solutions using novel alginate–iron oxide magnetic hydrogel composites. Polym.
578 Bull. 75, 5455–5475. https://doi.org/10.1007/s00289-018-2338-6

579 Soto, M.L., Moure, A., Domínguez, H., Parajó, J.C., 2011. Recovery, concentration and
580 purification of phenolic compounds by adsorption: A review. J. Food Eng. 105, 1–27.
581 https://doi.org/10.1016/J.JFOODENG.2011.02.010

582 Srinivasan, R., 2013. Green chemistry: challenges and opportunities, in: Mishra, A., Clark, J.H.
583 (Eds.), RSC Green Chemistry Series. Royal Society of Chemistry, Cambridge, pp. 51–81.

584 Stein, A., Wang, Z., Fierke, M.A., 2009. Functionalization of porous carbon materials with
585 designed pore architecture. Adv. Mater. 21, 265–293.

586 Subramanian, V., Zhu, H., Wei, B., 2008. Alcohol-assisted room temperature synthesis of
587 different nanostructured manganese oxides and their pseudocapacitance properties in
588 neutral electrolyte. Chem. Phys. Lett. 453, 242–249.
589 https://doi.org/10.1016/J.CPLETT.2008.01.042

590 Suhas, Gupta, V.K., Carrott, P.J.M., Singh, R., Chaudhary, M., Kushwaha, S., 2016. Cellulose:
591 A review as natural, modified and activated carbon adsorbent. Bioresour. Technol. 216,
592 1066–1076. https://doi.org/https://doi.org/10.1016/j.biortech.2016.05.106

593 Sun, J., Zhou, J., Shang, C., Kikkert, G.A., 2014. Removal of aqueous hydrogen sulfide by
594 granular ferric hydroxide-kinetics, capacity and reuse. Chemosphere 117, 324—329.
595 https://doi.org/10.1016/j.chemosphere.2014.07.086

596 Tamersit, S., Bouhidel, K.-E., 2020. Treatment of tannery unhairing wastewater using carbon
597 dioxide and zinc cations for greenhouse gas capture, pollution removal and water recycling.
598 J. Water Process Eng. 34, 101120.
599 https://doi.org/https://doi.org/10.1016/j.jwpe.2019.101120

600 Thompson, M.A., Kelkar, U.G., Vickers, J.C., 1995. The treatment of groundwater containing
601 hydrogen sulfide using microfiltration. Desalination 102, 287–291.
602 https://doi.org/10.1016/0011-9164(95)00065-A

603 Vaiopoulou, E., Melidis, P., Aivasidis, A., 2005. Sulfide removal in wastewater from
604 petrochemical industries by autotrophic denitrification. Water Res. 39, 4101–4109.
605 https://doi.org/10.1016/J.WATRES.2005.07.022

606 Valeika, V., Beleska, K., Valeikiene, V., 2006. Oxidation of Sulphides in Tannery Wastewater
607 by Use of Manganese (IV) Oxide. Polish J. Environ. Stud. 15, 623–629.

608 Wang, J., Guo, X., 2020. Adsorption kinetic models: Physical meanings, applications, and
609 solving methods. J. Hazard. Mater. 390, 122156.
610 https://doi.org/10.1016/J.JHAZMAT.2020.122156

Weber, W.J., Morris, C.J., 1963. Kinetics of Adsorption on Carbon from Solution. J. Sanit. Eng. Div. 89, 31–60.

Wilk, Ł.J., Ciechanowska, A., Kociołek-Balawejder, E., 2020. Removal of sulfides from water using a hybrid ion exchanger containing manganese(IV) oxide. Sep. Purif. Technol. 231, 115882. https://doi.org/https://doi.org/10.1016/j.seppur.2019.115882

Willey, B.F., Jennings, H., Muroski, F., 1964. Removal of Hydrogen Sulfide With Potassium Permanganate. J. Am. Water Work. Assoc. 56, 475–479. https://doi.org/10.1002/j.1551-8833.1964.tb01236.x

Yao, W., Millero, F.J., 1993. The rate of sulfide oxidation by δMnO2 in seawater. Geochim. Cosmochim. Acta 57, 3359–3365. https://doi.org/10.1016/0016-7037(93)90544-7

LIST OF FIGURES

(*Color print required*)

Fig. 1: Scanning Electron Microscopy (SEM) and EDX results of nanoparticle composites: (a-b) fresh MnO_2 (c-d) spent MnO_2 (e-f) Fresh MnO_2-PGC composite (g-h) sulfide adsorbed MnO_2-PGC composite.

Fig. 2: Transmission Electron Microscopy (TEM) images of synthesized (a) δ-MnO_2 and (b) MnO_2-PGC composite.

Fig. 3: X-ray diffractograms of various fresh and spent adsorbents.

Fig. 4: Effect of pH on sulfide removal using different adsorbents.

Fig. 5: Effect of adsorbent mass on sulfide removal using different adsorbents.

Fig. 6: Effect of initial sulfide solution concentration on sulfide removal using different adsorbents.

Fig. 7: Effect of contact time on removal efficiency and uptake capacity.

LIST OF TABLES

Table 1: Summary of kinetic model equations and parameters of PGC-MnO_2 composite

Table 2: Comparison of sulfide adsorption capacities for different adsorbents

LIST OF SUPPLEMENTARY SECTION

Fig. S1: Schematic of the adsorbent synthesis technique

Fig. S2: Effect of ionic strength on sulfide removal efficiency of MnO_2-PGC adsorbent

Fig. S3: Intra-particle diffusion models representing different phases in sulfide adsorption on MnO_2-PGC composite.

Fig. S4: Pseudo first and second order reaction models for sulfide adsorption on MnO_2-PGC composite.

Table S1: Parameters for different isotherm models at 298 K

Adsorptive oxidation of sulfides catalysed by δ-MnO_2 decorated porous graphitic carbon composite

Anjali Achazhiyath Edathil, Pravin Kannan*, Fawzi Banat

Department of Chemical Engineering, Khalifa University, Abu Dhabi, United Arab Emirates

Highlights

- δ-MnO_2/porous graphitic carbon nanocomposite synthesized by in-situ wet deposition
- Surface functionalized PGC and precipitated δ-MnO_2 catalyzed oxidation of sulfides
- Sulfides species converted to metal sulfates and sulfur, and removed by adsorption
- Equilibrium best-described by Langmuir model with an uptake capacity of 526.3 mg/g
- Kinetic intra-particle diffusion model suggested multiple rate-controlling steps

* Corresponding author. *Tel*.: +971 26075198

Email addresses: pravin.kannan@ku.ac.ae

Declaration of interests

☒ The authors declare that they have no known competing financial interests or personal relationships that could have appeared to influence the work reported in this paper.

☐The authors declare the following financial interests/personal relationships which may be considered as potential competing interests:

None